Control of focusing fields in laser-plasma accelerators using higher-order modes

E. Cormier-Michel,[1,*] E. Esarey,[1] C. G. R. Geddes,[1] C. B. Schroeder,[1] K. Paul,[2] P. J. Mullowney,[2]
J. R. Cary,[2] and W. P. Leemans[1]

[1]*Lawrence Berkeley National Laboratory, Berkeley, California 94720, USA*
[2]*Tech-X Corporation, Boulder, Colorado 80303, USA*

Higher-order laser modes are analyzed as a method to control focusing forces and improve the electron bunch quality in laser-plasma accelerators. In the linear wake regime, the focusing force is proportional to the transverse gradient of the laser intensity, which can be shaped by a superposition of modes. In particular, the transverse wakefield can be arbitrarily small in a region about the axis by adjusting the laser modes. Plasma channel effects, which prohibit the formation of the controlled-focusing region, can be mitigating by introducing a delay between the modes. Modes with parallel polarization produce a beat interference in the laser intensity, which lead to deflecting forces. This can be avoided by using modes with orthogonal polarization, different frequencies, or short pulses that do not overlap. Particle-in-cell simulations are performed of a laser-plasma accelerator in the quasilinear regime driven by high-order modes. Simulations show that, by including the first-order mode, the matched radius of the electron bunch is substantially increased, which for fixed bunch density and emittance implies an increase in the beam charge.

PACS numbers: 52.38.Kd, 52.38.Hb, 52.35.Mw, 41.75.Jv

I. INTRODUCTION

Guiding of intense laser pulses in plasma channels [1] has many applications, including x-ray lasers [2], high harmonic generation [3], and laser-plasma accelerators (LPAs) [4,5]. Propagation of high-order laser modes is also important for direct electron acceleration by the laser field in vacuum [6] and in plasma channels [7], and to improve injection schemes in LPAs [8]. Plasma channel applications rely on the propagation of the laser pulse at high intensity, up to 10^{19} W/cm^2 for laser-plasma accelerators [9], over long distances. In vacuum, a laser pulse of spot size r_0 diffracts over a distance of the order of the Rayleigh length $Z_R = \pi r_0^2/\lambda$, where λ is the laser wavelength. For intense pulses, the spot size is small and hence the laser diffracts rapidly, e.g., $Z_R = 250$ μm for $\lambda = 0.8$ μm and $r_0 = 10$ μm for a Gaussian pulse. Plasma channels, with a parabolic radial density profile $n(r) = n_0 + \Delta n r^2/r_0^2$, have the property of guiding a laser pulse of spot size r_0 over many Rayleigh lengths, provided that the channel depth satisfies $\Delta n = \Delta n_c = 1/\pi r_e r_0^2$ in the low laser intensity limit, where $r_e = e^2/mc^2$ is the classical electron radius. This has been experimentally demonstrated using plasma channels generated by hydrodynamic expansion [10,11] or capillary discharges [12–14]. Furthermore, plasma channels have been used to

*Presently at Tech-X Corporation, Boulder, CO 80303.

guide intense ($> 10^{18}$ W/cm^2) laser pulses in laser-plasma accelerator experiments [9,15]. High quality electron beams at the GeV level have been produced by guiding an intense laser pulse over a 3 cm plasma capillary waveguide [15]. These experiments have furthered the interest in using channel-guided LPAs to drive future electron-positron colliders [16].

In a LPA, the accelerating and focusing fields (wakefields) are driven by the ponderomotive force of the laser pulse $F \sim \nabla a^2$, where $a^2 = 7.2 \times 10^{-19}\lambda^2[\mu m]\times I[W/cm^2]$ is the normalized laser intensity (linear polarization) and $a = eA/mc^2$ is the normalized amplitude of the vector potential of the laser field. The accelerating fields can be 3 orders of magnitude greater than those in conventional accelerators. The magnitude of the focusing field, which is typically zero on axis, can approach that of the accelerating field off axis, depending on the laser spot size, laser intensity, and plasma density. Two typical regimes of operation [5] are presently being explored for wakefields driven by short laser pulses ($k_p L \lesssim 1$): the highly nonlinear blowout (or bubble) regime and the quasilinear (or standard) regime. Here L is the laser pulse length and $\omega_p = ck_p = 2\pi c/\lambda_p = (4\pi n e^2/m)^{1/2}$ is the plasma frequency with n the plasma density. In the blowout regime, typically characterized by $a^2 \sim (k_p r_0/2)^4 \gg 1$, the focusing field is maximum (determined by the ion column left behind the laser pulse) and is comparable in amplitude to the accelerating field [17,18], i.e., $E_z/E_0 \simeq k_p \zeta/2$ and $(E_r - B_\theta)/E_0 \simeq k_p r/2$, where $\zeta = z - ct$ (the center of the bubble is at $\zeta = 0$ and $r = 0$). In the linear or quasilinear regime, typically characterized by $a^2 \lesssim 1$, the electric fields of the wake are directly proportional to the

gradient of the intensity profile, i.e., $E_z \sim \partial a^2/\partial z$ and $E_\perp \sim \nabla_\perp a^2$. Hence, in the linear regime, the focusing force can be reduced by tailoring the transverse intensity profile of the laser pulse. For example, for a flattop transverse profile $a^2 = a_0^2$, $F_\perp \sim \nabla_\perp a^2 = 0$.

Large focusing forces in a plasma-based accelerator can be detrimental for several reasons. For example, large focusing forces can lead to large betatron oscillations of the accelerated electrons. This will produce betatron (synchrotron) radiation [19] that can increase the energy spread on the electron beam [20]. Furthermore, large focusing forces require that the matched beam radius of the accelerated electron beam be very small. The evolution of the rms radius of a highly relativistic electron beam σ_x is given by $d^2\sigma_x/dz^2 + k_\beta^2\sigma_x - \epsilon_n^2/\gamma^2\sigma_x^3 = 0$, assuming a linear focusing force ($F_x \sim x$), no acceleration, a narrow energy spread, and no space charge effects. Here, ϵ_n is the normalized emittance, γ is the relativistic factor, and k_β is the betatron wave number, which is related to the focusing force by $k_\beta^2 x = k_p(E_x - B_y)/\gamma E_0$. The condition for a matched (nonevolving) electron beam radius, which is desired for emittance preservation and minimization of radiation, is given by balancing the focusing and emittance terms, i.e., $\sigma_{xm} = (\epsilon_n/\gamma k_\beta)^{1/2}$. For example, in the blowout regime [17–19,21], where the focusing forces are maximum, the betatron wave number is $k_\beta = k_p/(2\gamma)^{1/2}$, and for $n = 10^{17}$ cm^{-3}, $\gamma = 2 \times 10^4$ (10 GeV), and $\epsilon_n = 1$ μm, the matched beam radius is $\sigma_x = 0.4$ μm. Such a small electron beam radius results in exceptionally stringent alignment and coupling tolerances between accelerator stages. In addition, a small beam radius can limit the charge in the accelerated bunch. For example, in the linear and quasilinear wake regimes a large beam density implies large beam loading [22], i.e., deformation of the accelerating fields, which can degrade beam quality. In the highly nonlinear wake (blowout) regime, a high beam density can cause ion motion, degrading the beam emittance [23].

In this paper we demonstrate reduction and control of the focusing forces in the quasilinear wakefield regime by using higher-order laser modes to shape the transverse intensity profile. We first consider the propagation of higher-order laser modes in a parabolic plasma channel. In Sec. II, solutions of the paraxial wave equation, in the low intensity limit and in the case of a matched laser pulse, are presented for different geometries. Issues due to the copropagation and beating of two laser modes are addressed. In Sec. III, analytical expressions for the transverse wakefield excited by a laser pulse with higher-order modes are derived, including corrections for a parabolic density profile, yielding conditions to reduce and shape the focusing forces. Particle-in-cell (PIC) simulations, with the code VORPAL [24], are then used to propagate an electron beam in a wakefield driven by high-order modes. Simulations in 2D indicate that, by using a laser transverse profile with a nearly flattop shape near axis, the matched

beam radius can be increased by a factor of ~3, without significant growth of the emittance, which, when extrapolated to 3D, corresponds to an increase of a factor of ~9 in charge. Methods for mitigating the effects of mode beating in laser-plasma accelerators are also discussed. In the Appendix, we show the accuracy of the numerical results of the PIC code by benchmarking with the particle tracking code general particle tracer (GPT) [25].

II. HIGHER-ORDER LASER MODES IN PLASMA CHANNELS

The basic properties of higher-order laser mode propagation in a plasma channel can be examined using the paraxial wave equation in the low intensity limit. First, propagation of a single mode in a plasma channel is considered. Two modes are discussed next, including the effects of mode beating, which occurs when the two modes have parallel polarizations.

A. Propagation of a single mode

The leading-order evolution of the slowly varying transverse envelope $\hat{a}_\perp$ of a low intensity ($|\hat{a}_\perp|^2 \ll 1$) laser pulse in a plasma channel of the form $n(r) = n_0 + \Delta n r^2/r_0^2$ is described by the paraxial wave equation [26],

$$\left(\nabla_\perp^2 + 2ik\frac{\partial}{\partial z}\right)\hat{a}_\perp = k_p^2\left(1 + \frac{\Delta n}{n_0}\frac{r^2}{r_0^2}\right)\hat{a}_\perp, \quad (1)$$

where $k = 2\pi/\lambda$ is the laser wave number and $k_p = \omega_p/c = (4\pi n_0 e^2/mc^2)^{1/2}$ is evaluated using the electron density on axis n_0. The full laser field is given by $a_{f\perp} = (\hat{a}_\perp/2)\exp[ik(z - ct)] +$ c.c., where the vector potential has been normalized $\boldsymbol{a}_f = e\boldsymbol{A}_f/mc^2$ and Coulomb gauge $\nabla \cdot \boldsymbol{a}_f = 0$ is assumed. The paraxial wave equation neglects short-pulse effects, such as longitudinal dispersive spreading of the laser pulse, which occurs over distances much longer than those of interest [27]. Nonlinear effects, such as plasma wave excitation and relativistic self-focusing, are also neglected.

In the following, solutions are considered for linearly polarized laser pulses in both cylindrical and Cartesian geometries, as well as radially polarized fields in cylindrical geometry. In addition to the structure of the higher-order mode, the phase velocity is also important, as is discussed below.

1. Linear polarization, cylindrical geometry

In cylindrical geometry (r, ϕ, z), solutions to the paraxial wave equation, Eq. (1), for a linearly polarized field $\hat{a}_\perp = \hat{a}_x$ are of the general form [27]:

$$\hat{a}_{x,(m,p)}(r,\phi,z) = a_{m,p}\frac{r_s}{r_0}(\sqrt{2}r/r_s)^p L_m^p(2r^2/r_s^2)$$
$$\times \exp[-(1-i\alpha_s)r^2/r_s^2 + i\theta_{m,p} + ip\phi], \tag{2}$$

where L_m^p is the generalized Laguerre polynomial and ϕ the polar angular coordinate. The quantities $\alpha_s(z)$, $r_s(z)$, and $\theta_{m,p}(z)$, which represent the curvature, the spot size, and the phase shift, respectively, satisfy

$$\alpha_s = \frac{kr_s}{2}\frac{\partial r_s}{\partial z}, \tag{3}$$

$$\frac{\partial^2 r_s}{\partial z^2} = \frac{4}{k^2 r_s^3}\left(1 - \frac{\Delta n}{\Delta n_c}\frac{r_s^4}{r_0^4}\right), \tag{4}$$

$$\frac{\partial \theta_{m,p}}{\partial z} = -\frac{1}{2k}\left[k_p^2 + \frac{4}{r_s^2}(2m+p+1)\right]. \tag{5}$$

The above Laguerre-Gaussian modes form a complete orthonormal set of basis functions and, hence, any arbitrary transverse profile $\hat{a}(r,\phi)$ can be expanded into a series of Laguerre-Gaussian modes. Since the evolution of each mode is known via the above equations, the evolution of $\hat{a}(r,\phi)$ is known via the sum of series expansions.

From Eq. (4), the condition for a matched (nonevolving) spot size $r_s(z) = r_0$ is that the channel depth satisfy $\Delta n = \Delta n_c$, where $\Delta n = 1/\pi r_e r_0^2$ is the critical channel depth. Notice that this condition is independent of mode number (m,p), i.e., the condition to guide a given mode at a matched spot $r_s = r_0$ is the same for all modes [27].

In the case of a matched spot size, i.e., $\Delta n = \Delta n_c$ and $r_s = r_0$, the solution can be written as

$$\hat{a}_{x,(m,p)}(r,\phi,z) = a_{m,p}(\sqrt{2}r/r_0)^p L_m^p(2r^2/r_0^2)$$
$$\times \exp(-r^2/r_0^2 + i\theta_{m,p} + ip\phi), \tag{6}$$

with $\alpha_s = 0$ and $\theta_{m,p} = (-1/2k)[k_p^2 + 4(2m+p+1)/r_0^2]z$. Note that the axisymmetric modes correspond to $p = 0$.

The phase shift $\theta_{m,p}(z)$ depends on the mode numbers (m,p), and hence the group and phase velocities do as well. The axial phase velocity is given by $\beta_{\rm ph} \simeq 1 - \Delta k/k$, where $\Delta k = \partial \theta_{(m,p)}/\partial z$ is the axial wave number shift. For the Laguerre-Gaussian modes

$$\beta_{\rm ph} \simeq 1 + \frac{1}{2k^2}\left[k_p^2 + \frac{4(2m+p+1)}{r_0^2}\right]. \tag{7}$$

Hence, higher-order modes will have a larger phase velocity. Even though two modes can be combined and propagated simultaneously in the same plasma channel, the difference in phase velocity will induce interference patterns and intensity modulations.

2. Linear polarization, Cartesian geometry

The solution can also be written in terms of Hermite-Gaussian modes in the Cartesian coordinate system (x, y, z). For the case of a matched spot in a plasma channel in three dimensions (3D),

$$\hat{a}_{x,(m,p)}(x,y,z) = \frac{a_{m,p}}{(m!p!2^{m+p})^{1/2}}H_m\left(\frac{\sqrt{2}x}{r_0}\right)H_p\left(\frac{\sqrt{2}y}{r_0}\right)$$
$$\times \exp[-(x^2+y^2)/r_0^2 + i\theta_{m,p}], \tag{8}$$

where H_m is the Hermite polynomial of order m and $\theta_{m,p} = (-1/2k)[k_p^2 + 4(m+p+1)/r_0^2]z$. The phase velocity for the Hermite-Gaussian modes is

$$\beta_{\rm ph} \simeq 1 + \frac{1}{2k^2}\left[k_p^2 + \frac{4(m+p+1)}{r_0^2}\right]. \tag{9}$$

In two dimensions (2D), the Hermite-Gaussian modes are given by

$$\hat{a}_{x(m)}(x,z) = \frac{a_m}{(m!2^m)^{1/2}}H_m(\sqrt{2}x/r_0)\exp(-x^2/r_0^2 + i\theta_m), \tag{10}$$

with $\theta_m = (-1/2k)[k_p^2 + 2(2m+1)/r_0^2]z$ and

$$\beta_{\rm ph} \simeq 1 + \frac{1}{2k^2}\left[k_p^2 + \frac{2(2m+1)}{r_0^2}\right]. \tag{11}$$

Note that $H_m(\sqrt{2}x/r_0)$ is not symmetric about $x = 0$ for odd values of m.

3. Radial polarization, cylindrical geometry

Solutions for radially symmetric, radially polarized modes in the cylindrical geometry (r, z) are given by

$$\hat{a}_{r,(m)}(r,z) = a_m\frac{r}{r_0}\left(\frac{2}{m+1}\right)^{1/2}L_m^1(2r^2/r_0^2)$$
$$\times \exp(-r^2/r_0^2 + i\theta_m), \tag{12}$$

assuming a matched spot size, with $\theta_m = -(1/2k)[k_p^2 + 8(m+1)/r_0^2]z$ and

$$\beta_{\rm ph} \simeq 1 + \frac{1}{2k^2}\left[k_p^2 + \frac{8(m+1)}{r_0^2}\right]. \tag{13}$$

Note that these modes have zero amplitude on axis $(r = 0)$.

4. Simulations

The above results are analytical solutions to the paraxial wave equation in the linear limit. To verify these solutions, and show self-consistent propagation, simulations were performed using the PIC code VORPAL [24]. Figure 1 shows the results for different linearly polarized laser modes in 2D Cartesian geometry (x, z), propagating in a plasma channel with a density on axis $n_0 = 10^{19}$ cm^{-3} and a channel depth satisfying the condition for matched propagation, $\Delta n = \Delta n_c = 1/\pi r_e r_0^2$. Figures 1(a) and 1(b) show
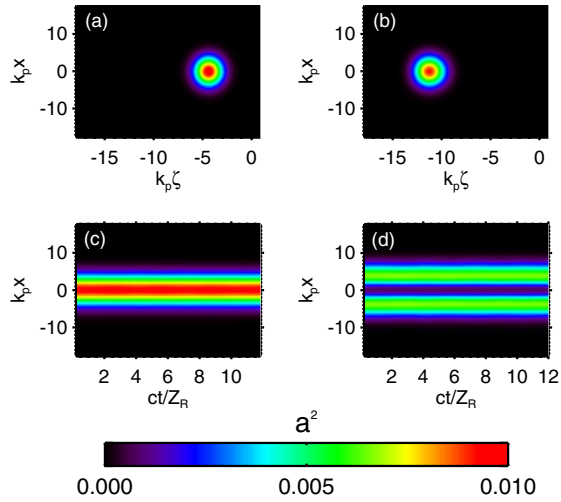
FIG. 1.   Normalized intensity profile as a function of longitudinal $k_p\zeta = k_p(z - ct)$ and transverse $k_p x$ coordinates, for the fundamental Gaussian mode propagating in a matched plasma channel, at (a) $ct/Z_R = 0.22$ and (b) $ct/Z_R = 10$ (slippage due to $v_g < c$ is visible); (c) corresponding transverse intensity profile, integrated over the longitudinal dimension, as a function of propagation distance. (d) Integrated transverse intensity profile of the first-order Hermite-Gaussian mode propagating in the same plasma channel.

the normalized intensity profile $|\hat{a}|^2$ versus $k_p x$ and $k_p\zeta$ for the fundamental Gaussian laser mode [Eq. (10) with $m = 0$] at $ct/Z_R = 0.2$ and $ct/Z_R = 10$, respectively, where $\zeta = z - ct$. Here, the initial mode parameters are a normalized amplitude of $a_0 = 0.1$, a normalized spot size of $k_p r_0 = 5.3$ ($Z_R = k_p r_0^2/2$ is the Rayleigh length), and a normalized pulse length of $k_p L = 2$, where the longitudinal intensity profile is assumed to be a Gaussian of the form $a^2 \sim \exp(-2\zeta^2/L^2)$. Figures 1(a) and 1(b) show that the mode shape stays constant both longitudinally and transversely over many Rayleigh lengths. The slippage in $k_p\zeta$ is due to the group velocity of the laser in the plasma that is less than c. Figure 1(c) shows the transverse pulse profile integrated over the longitudinal dimension $k_p\zeta$, which determines the plasma response, of the fundamental Gaussian laser pulse as a function of propagation distance ct/Z_R. Figure 1(d) shows the evolution of the first-order Hermite-Gaussian mode [Eq. (10) with $m = 1$], with $a_1 = 0.1$, $k_p r_0 = 5.3$, and $k_p L = 2$, propagating in the same density channel. The two pulses can be guided independently in the same plasma channel over many Rayleigh lengths, without variations in the spot size, consistent with the theoretical prediction.

B. Propagation of two modes

The copropagation of two laser modes in the same plasma channel is considered next, which will allow the combination of different laser modes to tailor the laser intensity profile and, hence, the plasma wakefield. When adding two modes with the same polarization and the same frequency, the time-averaged intensity profile becomes

$$\langle[a_{fx}(m_0, p_0) + a_{fx}(m_1, p_1)]^2\rangle$$
$$= \frac{a_{m_0,p_0}^2}{2} + \frac{a_{m_1,p_1}^2}{2} + a_{m_0,p_0}a_{m_1,p_1}\cos(\theta_{m_0,p_0} - \theta_{m_1,p_1}),$$

(14)

where angular brackets denote a time average over the fast laser frequency. For linear polarized, Laguerre-Gaussian modes in cylindrical geometry,

$$\theta_{m_0,p_0} - \theta_{m_1,p_1} = k_{\text{beat}}z = [(2m_1 + p_1) - (2m_0 + p_0)]z/Z_R,$$

(15)

where $\lambda_{\text{beat}} = 2\pi/k_{\text{beat}}$ is the beat wavelength. The cross term induces an oscillation of the intensity profile. Because the phase shift and the phase velocity are different for different modes, the intensity profile of the laser is modulated if two copropagating modes have parallel polarization. For example, for the fundamental ($m_0 = 0$, $p_0 = 0$) and m^{th}-order cylindrically symmetric ($m_1 = m$, $p_1 = 0$) Laguerre-Gaussian modes, the beat wave number is $k_{\text{beat}} = 2m/Z_R$. To avoid this envelope modulation the two modes must be orthogonally polarized; in that case the time-averaged intensity profile is given by $\langle[a_{fx}(m_0, p_0) + a_{fy}(m_1, p_1)]^2\rangle = a_{m_0,p_0}^2/2 + a_{m_1,p_1}^2/2$, i.e., there is no cross term.

Figure 2 shows the result of 2D PIC simulations when copropagating the fundamental Gaussian mode ($a_0 = 0.1$) and the first-order Hermite-Gaussian mode ($a_1 = 0.1$). The pulse propagates in a matched plasma channel with an on-axis density $n_0 = 10^{19}$ cm^{-3} and both modes have $k_p r_0 = 5.3$ and $k_p L = 2$. Figures 2(a) and 2(b) show the intensity profile at $ct/Z_R = 0.2$ and $ct/Z_R = 10$, respectively, when the two modes have parallel polarization showing the intensity oscillations. Figure 2(c) shows the corresponding integrated transverse intensity profile, as a function of propagation distance, modulated at a wave number $1/Z_R$. In Fig. 2(d), however, the two modes are orthogonally polarized and the transverse intensity profile stays constant over many Rayleigh lengths.

Additional 2D PIC simulations show that the mode propagation behaves similarly at intensities relevant to the quasilinear regime of the laser wakefield accelerator [22,28]. As an example, Fig. 3 shows the integrated intensity profile ($\sim \int d\zeta|E|^2$) of the cross-polarized fundamental Gaussian and first-order Hermite-Gaussian modes with $a_0 = 0.7$ and $a_1 = 0.5$. To compensate for the self-focusing of the laser pulse, the channel depth is adjusted such that $\Delta n = 0.7\Delta n_c$, which minimized oscillations of the laser spot size. The two modes are guided over many Rayleigh lengths in this same plasma channel without intensity modulation. During propagation, the laser depletes its energy and self-steepens [29], which results in a decrease of the value of the integrated intensity.
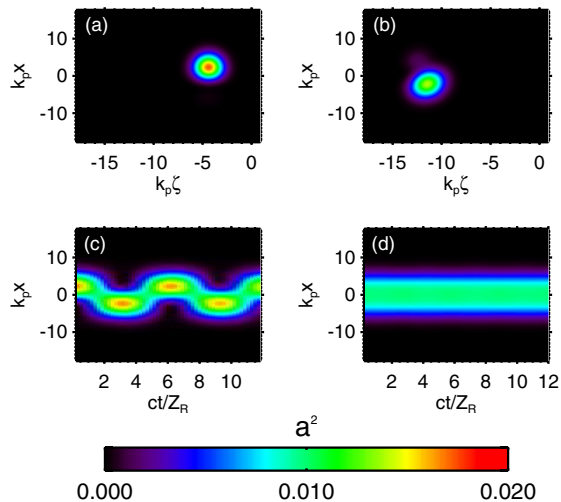
FIG. 2.   Normalized intensity profile as a function of longitudinal $k_p\zeta = k_p(z - ct)$ and transverse k_px coordinates, for a fundamental Gaussian plus a first-order Hermite-Gaussian mode, with the same polarization, propagating in a matched plasma channel in 2D Cartesian geometry, at (a) $ct/Z_R = 0.22$ and (b) $ct/Z_R = 10$; (c) corresponding transverse intensity profile, integrated over the longitudinal dimension, as a function of propagation distance. (d) Integrated transverse intensity profile of the two modes with cross-polarization.
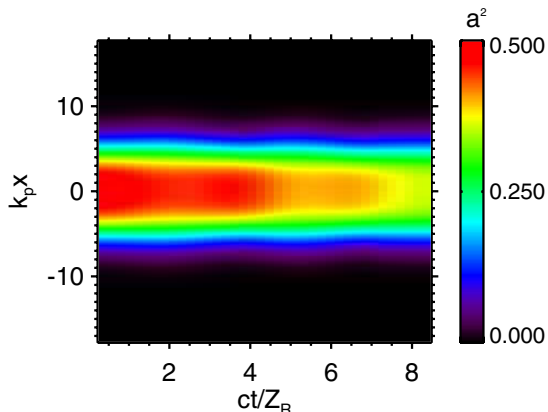
FIG. 3.   Integrated transverse intensity profile of a Gaussian and Hermite-Gaussian ($m = 1$) pulse with orthogonal polarization, as a function of propagation distance, with $a_0 = 0.7$ and $a_1 = 0.5$.

The laser transverse shape remains constant, however, keeping the transverse wake structure constant.

In three dimensions (3D), using two modes to create a near flattop transverse intensity profile near axis [similar to that shown in Fig. 2(d)] is problematic, since beating of the modes is difficult to avoid. For example, suppose that an axisymmetric profile is created by adding a linearly polarized fundamental Gaussian mode, $a_{0,0} \exp(-r^2/r_0^2 + i\theta_{0,0})e_x$, with a radially polarized mode, $a_0\sqrt{2}(r/r_0)\times L_0^1(2r^2/r_0^2) \exp(-r^2/r_0^2 + i\theta_0)e_r$. Along the y axis

there is no beating, but along the x axis the modes beat, producing an intensity modulation similar to that shown in Fig. 2(c).

For LPAs, however, the beating of modes can be mitigated using a variety of methods. For example, the wake can be driven by using two short pulses (e.g., the lowest-order linear polarized mode and the lowest-order radially polarized mode, both with $k_pL \lesssim 2$) that are longitudinally separated by a multiple of the plasma period $2\pi/\omega_p$ (the use of multiple laser pulses in 1D to enhance the wake amplitude is considered in Refs. [30,31]). The pulses do not physically overlap, so there is no beating, but the wakefield behind the second pulse will have the structure of that driven by the sum of the intensity profiles of the two separate pulses [5]. Another method for mitigating the beating between modes in LPAs is to use two modes with different frequencies such that the beat frequency is much greater than the plasma frequency. These methods will be discussed in more detail in the following sections.

Designs for future electron-positron colliders may require the use of highly elliptical particle beams, with aspect ratios on the order of 100 [32]. One possibility for a future collider based on LPAs is to use a similarly highly elliptical drive laser. In this case the laser-plasma geometry is essentially a slablike, Cartesian geometry. Two Hermite-Gaussian laser modes could be used to control the focusing forces, with orthogonal polarization, such that mode beating is avoided.

III. APPLICATION TO LASER-PLASMA ACCELERATORS

As discussed in the Introduction, control and/or reduction of the focusing forces can be beneficial to LPAs. In the linear wake regime, the focusing forces are proportional to the transverse gradients in the laser intensity profile. Control of the focusing forces can be achieved by tailoring the transverse intensity profile using high-order modes. In the following we will consider the Gaussian mode and the first-order Hermite-Gaussian mode with orthogonal polarization in 2D. Generalization to 3D is straightforward with the methods described in Sec. III D.

A. Transverse wakefield response

In the linear wake regime [4], $a^2 \ll 1$, the wake response is determined by the normalized electrostatic potential, $\phi = e\Phi/mc^2$, governed by $(\partial^2/\partial t^2 + \omega_p^2)\phi = \omega_p^2 a^2/2$. In terms of the independent variable $\zeta = z - ct$,

$$\phi = k_p \int_{\zeta_0}^{\zeta} d\zeta' \sin[k_p(\zeta - \zeta')]|\hat{a}(\zeta')|^2/4, \quad (16)$$

where ζ_0 is in front of the laser pulse, and the additional factor of $1/2$ is from averaging the linear polarized laser fields over the fast laser oscillation. For a Gaussian longitudinal profile, $|\hat{a}(\zeta, x)|^2 = |\hat{a}(x)|^2 \exp(-2\zeta^2/L^2)$,

the expression of the wakefield potential behind the driver is

$$\phi = -|\hat{a}(x)|^2\sqrt{\pi/2}(k_pL/4)\exp(-k_p^2L^2/8)\sin(k_p\zeta). \quad (17)$$

Consider the intensity profile of two orthogonally polarized laser modes in 2D, as shown in Fig. 2(d),

$$\hat{a}^2(x) = a_0^2\exp(-2x^2/r_0^2) + (a_1^2/2)$$
$$\times \exp(-2x^2/r_0^2)[H_1(\sqrt{2}x/r_0)]^2, \quad (18)$$

with $H_1(\sqrt{2}x/r_0) = 2\sqrt{2}x/r_0$. The transverse electric field is given by $E_x/E_0 = -(1/k_p)\nabla_x\phi$, which, for $\hat{a}^2(x)$ given by Eq. (18) and assuming that k_p is constant (i.e., a uniform density profile), gives

$$E_x/E_0 = \phi_0 a_0^2\frac{4x}{k_pr_0^2}\left(1 - \frac{\alpha}{2} + \alpha\frac{x^2}{r_0^2}\right)\exp\left(-\frac{2x^2}{r_0^2}\right)\sin(k_p\zeta),$$
$$(19)$$

with $\phi_0 = \sqrt{\pi/2}(k_pL/4)\exp(-k_p^2L^2/8)$, and $\alpha = 4a_1^2/a_0^2$. By changing the ratio a_1/a_0, one can change the transverse gradient of E_x/E_0. In particular, $E_x/E_0 = 0$ near axis ($x^2/r_0^2 \ll 1$) for $a_1/a_0 = 1/\sqrt{2}$.

(a)

(b)

a_1/a_0	
0	
0.5	
0.7	
1	
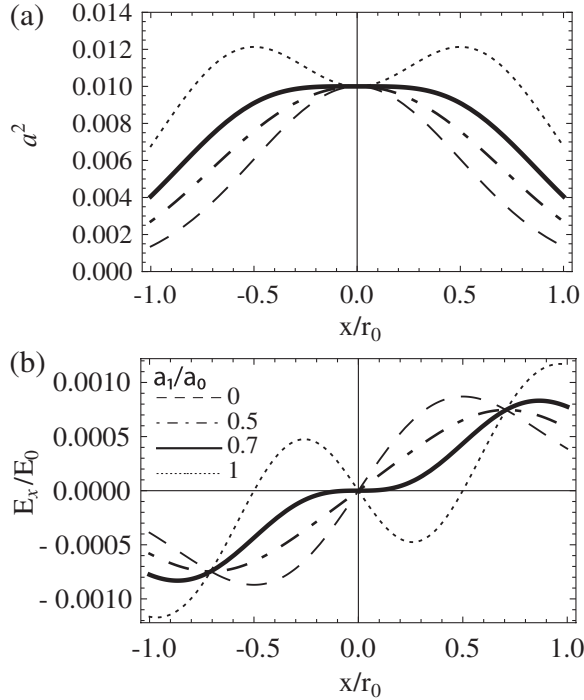
FIG. 4. (a) Transverse intensity profile when adding a fundamental Gaussian mode of normalized intensity $a_0 = 0.1$ and a first-order Hermite-Gaussian mode of normalized intensity a_1, with cross polarization, and (b) corresponding transverse electric field (obtained from theory neglecting the plasma channel) at $k_p\zeta = -\pi/2$, for $a_1/a_0 = 0$ (dashed line), $a_1/a_0 = 0.5$ (dash-dotted line), $a_1/a_0 = 1/\sqrt{2}$ (solid line), and $a_1/a_0 = 1$ (dotted line).
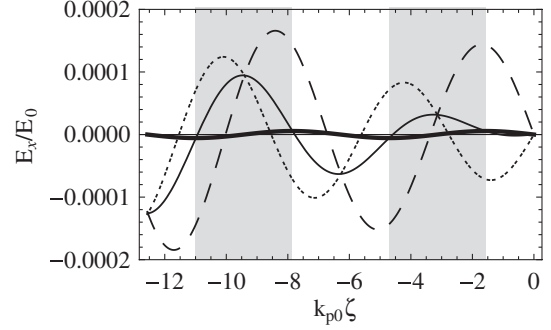
FIG. 5. Transverse electric field at $x/r_0 = 0.1$ driven by the Gaussian and Hermite-Gaussian pulses calculated in a matched plasma channel for $a_1/a_0 = 0.5$ (dashed line), $a_1/a_0 = 1/\sqrt{2}$ (solid line), and $a_1/a_0 = 0.8$ (dotted line). For comparison the transverse electric field calculated without the contribution of the plasma channel is shown for $a_1/a_0 = 1/\sqrt{2}$ (bold solid line), i.e., for a flattop intensity profile near axis as shown in Fig. 4. The gray areas indicate the accelerating region for electrons ($E_z < 0$).

Figures 4(a) and 4(b) show, respectively, the transverse intensity profile given by Eq. (18) and the corresponding transverse electric field E_x/E_0 given by Eq. (19) at the phase where the field is maximum ($k_p\zeta = -\pi/2$) for different values of a_1/a_0, with $k_pL = 2$, $k_pr_0 = 5.3$, and $a_0 = 0.1$. As a_1/a_0 increases the slope of the focusing field near axis decreases, and changes sign at $a_1/a_0 = 1/\sqrt{2}$, corresponding to the appearance of a dip in the intensity profile. Note that for $a_1/a_0 = 1/\sqrt{2}$ the focusing field near the axis is zero for all phases $k_p\zeta$ (see Fig. 5). The corresponding accelerating field is given by $E_z/E_0 = (-1/k_p)\nabla_z\phi = \phi_0\hat{a}^2(x)\cos(k_p\zeta)$, hence the transverse profile of the longitudinal wakefield is proportional to the laser intensity profile shown in Fig. 4(a). Because the gradient of the transverse field can be reduced and controlled near the axis by adjusting the relative intensity of the two modes, this allows control of the matched beam size for a given emittance.

B. Mitigation of plasma channel effects

The above calculation of the transverse wakefield neglected the presence of the density channel. The plasma channel, however, introduces a curvature in the transverse profile of the wakefield. Hence, the condition described above to have a flat transverse field near axis is more complicated when the effects of the channel are included. The effect of the transverse plasma density profile on the focusing field can be evaluated, to first approximation assuming a broad channel ($k_p^2r_0^2 \gg 1$), by using $k_p = k_p(x) = k_{p_0}(1 + \Delta nx^2/n_0r_0^2)^{1/2}$ in Eq. (17) [33], giving

$$\frac{E_x}{E_0} = \frac{-a_0^2L}{4r_0}\sqrt{\frac{\pi}{2}}\exp(-k_{p_0}^2L^2/8)\left(A_1\frac{x}{r_0} + A_3\frac{x^3}{r_0^3} + \cdots\right), \quad (20)$$

$$A_1 = \left(4 - \frac{\Delta n}{n_0} + \frac{k_{p_0}^2 L^2}{4} \frac{\Delta n}{n_0} - 2\alpha\right)\sin(k_{p_0}\zeta)$$
$$- \frac{\Delta n}{n_0} k_{p_0}\zeta \cos(k_{p_0}\zeta), \tag{21}$$

$$A_3 = -\left(8 - 4\frac{\Delta n}{n_0} + \frac{\Delta n}{n_0}k_{p_0}^2 L^2 - \frac{1}{2}\frac{\Delta n^2}{n_0^2} - \frac{\Delta n^2}{n_0^2}\frac{k_{p_0}^2 L^2}{4}\right.$$
$$+ \frac{1}{32}\frac{\Delta n^2}{n_0^2}k_{p_0}^4 L^4 - 8\alpha + 2\alpha\frac{\Delta n}{n_0}$$
$$\left. - \alpha\frac{\Delta n}{n_0}\frac{k_{p_0}^2 L^2}{2} - \frac{1}{2}\frac{\Delta n^2}{n_0^2}k_{p_0}^2\zeta^2\right)\sin(k_{p_0}\zeta)$$
$$+ \left(4\frac{\Delta n}{n_0} - \frac{1}{2}\frac{\Delta n^2}{n_0^2} + \frac{\Delta n^2}{n_0^2}\frac{k_{p_0}^2 L^2}{4}\right.$$
$$\left. - 2\alpha\frac{\Delta n}{n_0}\right)k_{p_0}\zeta \cos(k_{p_0}\zeta), \tag{22}$$

where $\Delta n_c x^2/n_0 r_0^2 = 4x^2/k_p^2 r_0^4 \ll 1$ has been assumed and terms of order x^5/r_0^5 have been neglected. Some effects of the plasma channel include the amplitude of the focusing field increasing as a function of distance behind the laser pulse $|\zeta|$, and the phase between the longitudinal and the transverse field varying as a function of $|\zeta|$ such that there is a greater overlap between the accelerating and focusing phase regions of the wake, the greater the distance behind the laser pulse [33]. Also neglected in the above expressions are terms of order $\zeta^2/k_p^2 r_0^4$, which can lead to a decrease in the amplitude of the longitudinal field with distance behind the laser pulse [33].

One consequence of the phase front curvature of the wake (caused by the density profile of the plasma channel) is that there is no condition on a_1/a_0 for which the transverse electric field is constant near axis for all phases $k_p\zeta$, as there was previously for a uniform plasma profile. Figure 5 shows the transverse electric field without (bold solid line) and with (solid line) the contribution of the plasma channel for $a_1/a_0 = 1/\sqrt{2}$, and $\Delta n/n_0 = 0.14$, corresponding to a matched spot size of $k_p r_0 = 5.3$. Whereas the transverse wakefield calculated for a uniform plasma profile is near zero for any phase at $x/r_0 = 0.1$ (the amplitude is of the order of 5×10^{-6} due to higher-order corrections in x/r_0), this is no longer true when including the contribution of the parabolic plasma profile. The condition for the gradient of the transverse electric field in the plasma channel to be controlled to an arbitrary value (e.g., zero) depends on $k_{p0}\zeta$ and is given by setting the sum of the first-order terms in x/r_0 to a specified value ($A_1 = $ constant), which gives

$$4 - 2\alpha - \frac{\Delta n}{n_0} + \frac{k_{p_0}^2 L^2}{4}\frac{\Delta n}{n_0} - \frac{\Delta n}{n_0}k_{p_0}\zeta \cos(k_{p_0}\zeta)/\sin(k_{p_0}\zeta)$$
$$= \text{constant}. \tag{23}$$

For example, setting the above equation to zero determines the phase $k_{p_0}\zeta$ where the transverse field gradient crosses the axis (for small x/r_0). Note that this phase depends on the ratio of the two mode intensities $\alpha = 4a_1^2/a_0^2$, i.e., the position of the focusing and defocusing region can be controlled by changing the ratio a_1/a_0. Figure 5 shows the transverse electric field, calculated in the plasma channel, for different values of α, at $x/r_0 = 0.1$. The minimal amplitude for the transverse field is still obtained for $a_1/a_0 = 1/\sqrt{2}$, but, because of the curvature of the channel, is no longer zero for all phases. The overlap between the focusing region of the transverse field $[E_x(x > 0)/E_0 > 0]$ and the accelerating region of the longitudinal electric field $(E_z/E_0) < 0$ (showed by the gray areas) depends on the relative intensity of the two modes.

For a LPA in the linear regime, driven with a single fundamental Gaussian mode in a uniform plasma, the overlap between the focusing and the accelerating field is $\lambda_p/4$. With a single fundamental Gaussian laser in a plasma channel, the overlap between the two regions can be increased to $\sim\lambda_p/2$, several plasma buckets after the laser pulse [33]. When using two laser modes in a plasma channel, as discussed above, an overlap of $\lambda_p/2$ between the focusing and the accelerating region can be achieved immediately after the laser pulse by adjusting the relative intensity of the two modes. Similarly, a focusing and accelerating region for a positron beam $[E_x(x > 0)/E_0 < 0$ and $E_\zeta/E_0 > 0]$ of width $\lambda_p/2$ can also be obtained for a specific ratio a_1/a_0.

To increase the electron beam spot size for a fixed emittance requires that the transverse electric field be reduced near axis. For an electron bunch of finite duration, it is beneficial that the transverse gradient of the focusing force be reduced and constant near the axis over a finite region of longitudinal phase $k_p\zeta$, which extends over a distance at least as long as the length of the electron bunch. This allows the matched beam radius to be uniform throughout the electron bunch and can reduce the variations in the focusing force as the beam dephases. A possible solution consists of time shifting the laser modes. Consider the response due to the Gaussian driver and that due to the first-order Hermite-Gaussian mode individually. For example, near the axis (to first order in x/r_0), the axial position (phase) at which the transverse wakefield is zero for the each mode occurs at different phases. The condition

$$\left(4 - \frac{\Delta n}{n_0} + \frac{k_{p_0}^2 L^2}{4}\frac{\Delta n}{n_0}\right)\sin(k_{p_0}\zeta_o) - \frac{\Delta n}{n_0}k_{p_0}\zeta_o\cos(k_{p_0}\zeta_o) = 0 \tag{24}$$

gives the phase $k_{p_0}\zeta_o$ for which the transverse wakefield due to the Gaussian pulse is zero near the axis, and

$$\sin(k_{p_0}\zeta_{o'}) = 0 \tag{25}$$

gives the phase $k_{p_0}\zeta_{o'}$ for which the transverse wakefield due the Hermite-Gaussian mode only is zero near the axis. The longitudinal position of the higher-order mode with respect to the fundamental can then be shifted by $\zeta_s = \zeta_{o'} - \zeta_o$ to align the two zero points. The condition on the ratio a_1/a_0 for which the transverse field gradient is set to an arbitrary constant (e.g., zero) over a small portion of phase surrounding this zero point can be calculated by linearly expanding the resulting expression of the transverse electric field around the zero point. As before, using only the term of first order in x/r_0, we set $A_1 =$ constant and expand in $\delta\zeta$ about ζ_o, i.e.,

$$
A_1 = \left(4 - \frac{\Delta n}{n_0} + \frac{k_{p_0}^2 L^2}{4}\frac{\Delta n}{n_0}\right)\sin(k_p\zeta_o + k_p\delta\zeta)
$$
$$
- \frac{\Delta n}{n_0}(k_p\zeta_o + k_p\delta\zeta)\cos(k_p\zeta_o + k_p\delta\zeta)
$$
$$
- 2\alpha\sin[k_p(\zeta_o + \zeta_s) + k_p\delta\zeta] = \text{constant}, \qquad (26)
$$

with $k_p\delta\zeta \ll 1$. The zeroth-order term ($\delta\zeta$ independent) is zero due to the definitions of ζ_o, $\zeta_{o'}$, and ζ_s. The first-order term in $\delta\zeta$ is then set to an arbitrary constant, for example zero, by

$$
\left(4 - 2\frac{\Delta n}{n_0} + \frac{k_{p_0}^2 L^2}{2}\frac{\Delta n}{n_0}\right)\cos(k_p\zeta_o) + \frac{\Delta n}{n_0}k_{p_0}\zeta_o\sin(k_p\zeta_o)
$$
$$
- 2\alpha\cos[k_p(\zeta_o + \zeta_s)] = 0, \qquad (27)
$$

which defines a value for α since $k_p\zeta_o$ and $k_p\zeta_s$ are known.

Figure 6(a) shows the contribution to the transverse field of the Gaussian, with $a_0 = 0.1$, and the Hermite-Gaussian mode, with $a_1 = a_0/\sqrt{2}$, separately and added together, for $k_{p_0}L = 2$ and $k_{p_0}r_0 = 5.3$. In Fig. 6(b) the Hermite-Gaussian mode has been shifted by $k_{p_0}\zeta_s = 0.33$, so the two curves cross the axis at the same point $k_{p_0}\zeta_o = -9.75$. The amplitude of the Hermite-Gaussian mode is then adjusted according to Eq. (27) ($a_1 = 0.73a_0$), so the resulting transverse field is zero (to first order) near the crossing point. One can then shape the focusing field longitudinally by adjusting the delay between the two modes and their relative amplitude. The sign of the field could, for example, be inverted locally or the slope set to different values, as needed to control beam propagation and compensate for beam loading.

Figure 7 shows the result of a 2D PIC simulation where a fundamental Gaussian pulse and a first-order Hermite-Gaussian pulse are added with crossed polarization, with $a_0 = 0.1$ (intensity of the fundamental Gaussian) and $a_1 = 0.73a_0$ (intensity of the higher-order mode), the latter being delayed by $k_{p_0}\zeta_s = 0.42$ compared to the fundamental. Note that the delay ($k_{p_0}\zeta_s = 0.42$) had to be slightly adjusted compared to the theoretical value ($k_{p_0}\zeta_s = 0.33$). Both modes have $k_{p_0}r_0 = 5.3$ and $k_{p_0}L = 2$. Figures 7(a) and 7(b) show the resulting longitudinal (dashed line) and transverse (solid line) fields after 400 μm and 2.4 mm
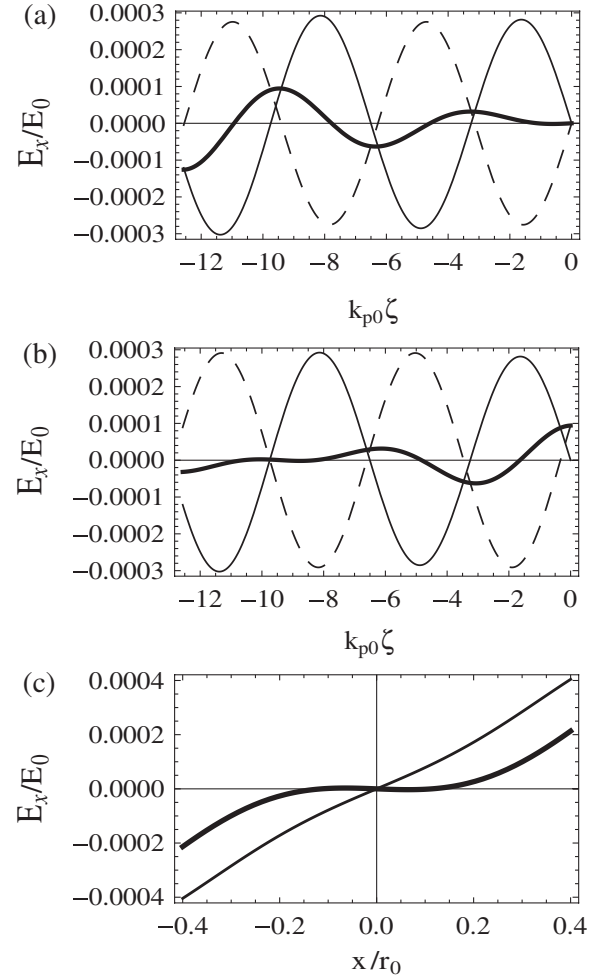
FIG. 6. Transverse electric field, at $x/r_0 = 0.1$. (a) The field from the Gaussian ($a_0 = 0.1$) only (dashed line) is shown as well as the field from the first-order Hermite-Gaussian mode ($a_1 = a_0/\sqrt{2}$) only (dotted line), and the sum (solid line). (b) The field from the Gaussian ($a_0 = 0.1$) only (dashed line) is shown as well as the field from the first-order Hermite-Gaussian mode (dotted line) shifted by $k_{p_0}\zeta_s = 0.33$ ($a_1 = 0.73a_0$) such that the sum (solid line) is $\simeq 0$, given $k_{p_0}\zeta_o = -9.75$. (c) Sum of the Gaussian and the first-order Hermite-Gaussian modes transversely at $k_{p_0}\zeta = -9$, with $a_0 = 0.1$ and $a_1 = 0.73a_0$, when the peaks of the two modes are aligned (thin line) and when the higher-order mode is shifted by $k_p\zeta_s = 0.33$ (thick line).

of propagation, respectively, in a matched plasma channel with a density on axis of $n_0 = 5 \times 10^{18}$ cm^{-3}. For comparison, the resulting transverse field when the higher-order mode is not delayed ($k_{p_0}\zeta_s = 0$) is also shown (dotted line). After 2.4 mm (corresponding approximately to half a dephasing length L_d, where $L_d \simeq \lambda_p^3/\lambda^2$), the focusing field is no longer zero, at the same phase it was zero initially, but still 2 times smaller than the corresponding field driven by the two modes without delay. Because the two modes have different group velocity, the delay between the two modes is changed by $k_{p_0}\Delta\zeta = k_{p_0}d(2/k^2r_0^2)$ for $m = 0$ and $m = 1$ in 2D, as the
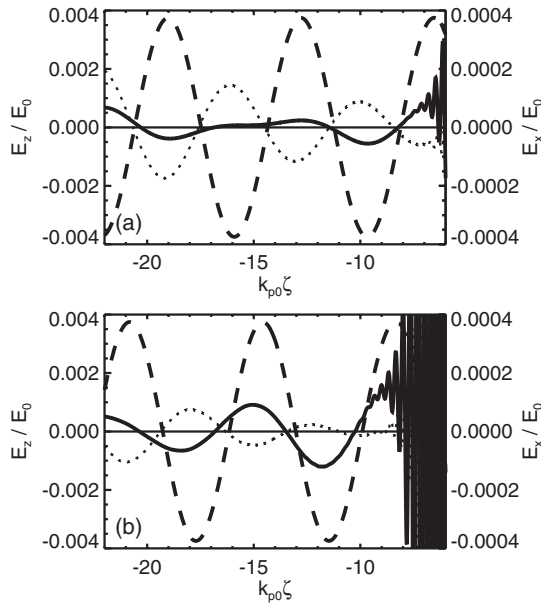
FIG. 7. 2D PIC simulation results showing the longitudinal (dashed line) and transverse (solid line) electric field driven by a fundamental Gaussian and first-order Hermite-Gaussian modes added with cross polarization, with $a_0 = 0.1$ and $a_1 = 0.73a_0$, the higher-order mode having a delay of $k_{p_0}\zeta_s = 0.42$, after (a) 400 μm and (b) 2.4 mm of propagation. The fields are plotted at $x/r_0 = 0.1$. For comparison the focusing field driven by the two modes, without delay, is also shown (dotted line).

FIG. 8. Results of 2D PIC simulations of a test electron beam propagating in a wakefield driven by a Gaussian mode only [thick solid line (magenta)], a Gaussian plus a Hermite-Gaussian mode [dashed line (blue)], and a Gaussian plus a Hermite-Gaussian mode, delayed by $k_{p_0}\zeta_s = 0.2$ [dash-dotted (black)]. (a) Energy gain, (b) evolution of the radius of the electron beam as a function of propagation distance, the dotted line shows the evolution of an unmatched beam in a wakefield driven by a Gaussian pulse, and (c) evolution of the beam emittance, $|\epsilon_n - \epsilon_{n0}|/\epsilon_{n0}$, with $\epsilon_{n0} = 0.014$ mm mrad.

pulse propagates over a distance d, i.e., the delay between the two modes is $k_{p_0}\zeta_s \simeq 0.66$ after $d = 2.4$ mm ($k_{p_0}d \simeq 1050$) and $k_{p_0}\zeta_s \simeq 0.87$ after $d = 5$ mm, leading to the evolution of the focusing field shape. Note that at lower density (lower k_{p_0}), the slippage is less for the same normalized propagation distance $k_{p_0}d$. One could adjust the delay initially so the electron beam stays in a focusing phase during the whole acceleration distance.

C. Electron bunch evolution

Particle-in-cell simulations were used to study the evolution of an externally injected test (i.e., no charge) electron bunch in the quasilinear regime ($a_0 = 1$), relevant to the design of efficient LPA stages [22,28]. In this regime the laser power is close to the critical power for self-focusing (for optimal spot sizes in this regime, $k_p r_0 \simeq 5$ [28]) and the laser pulse starts to evolve, although mildly, as it propagates into the plasma, i.e., undergoes self-focusing, depletion, and steepening. To reduce the effects of self-focusing and minimize the spot oscillations, the laser length is reduced to $k_p L = 1$ and a shallower plasma channel is used, such that $\Delta n \simeq 0.7\Delta n_c$. Furthermore, a laser pulse length of $k_p L = 1$ can also improve accelerator efficiency in the quasilinear regime [22]. A test electron beam, initially of zero length, is loaded in the accelerating and focusing region of the wakefield in the second bucket after the laser driver, and its evolution is followed as it

is accelerated in the wake. The transverse modes are adjusted as described above to shape the transverse field profile, the goal being to increase the matched electron beam radius for a given emittance, and to demonstrate that the latter is being conserved.

Figure 8 shows the evolution of the electron beam energy γ, radius σ_x, and of the emittance change $|\epsilon_n - \epsilon_{n0}|/\epsilon_{n0}$, where $\epsilon_{n0} = 0.014$ mm mrad ($k_p\epsilon_{n0} = 6 \times 10^{-3}$) is the initial normalized rms emittance, as a function of propagation distance for a Gaussian mode (solid line), a Gaussian plus a first-order Hermite-Gaussian mode with cross polarization (dashed line), and a Gaussian and Hermite-Gaussian mode, with cross polarization, delayed by $k_p\zeta_s = 0.2$ (dash-dotted line), propagating in a plasma channel with a density on axis $n_0 = 5 \times 10^{18}$ cm^{-3}. Because $k_p L = 1$ in this case the delay between modes to achieve a flat focusing field is different than that shown in

the previous section. The simulation box is 67×82 μm with 4000×614 cells and four particles per cell for the background plasma. In all cases, the beam is initially located at the same phase of the accelerating field, leading to same energy gain [Fig. 8(a)].

As seen in Fig. 8, the electron beam radius, for the Gaussian laser pulse case, is launched at the matched size $\sigma_x = 0.12$ μm and oscillates around $\sigma_x \simeq 0.1$ μm ($k_p \sigma_x \simeq 0.042$) $\pm 30\%$, with a normalized emittance of $\epsilon_n = 0.014$ mm mrad. The variation of the emittance is very small, about 0.01%. By using the Hermite-Gaussian mode, with $a_1 = 0.69 a_0$ in addition to the fundamental Gaussian pulse, the matched electron beam spot size can be increased to $\sigma_x \simeq 0.17$ μm. In this case, as the beam dephases it slips into the defocusing region of the transverse field, leading to an increase of the beam radius. It is found that by using $a_1 = 0.7 a_0$ the beam dephases sooner into the defocusing region, and the beam radius undergoes more variations, indicating that the beam evolution is very sensitive to small variations of the pulse intensity. If the acceleration is stopped at $ct = 2$ mm, the beam spot size varies by $\pm 5\%$ with 96% of the maximum energy, and again a very small variation of the emittance ($\simeq 0.01\%$). Finally, by using a delay of $k_p \zeta_s = 0.2$ between the two modes, with $a_1 = 0.69 a_0$, the matched beam radius is increased further to $\sigma_x \simeq 0.285$ μm and the variation decreased to $\pm 1.5\%$, for $ct < 2$ mm, which is almost a factor of 3 increase in radius compared to the fundamental Gaussian only. As shown in Fig. 8(b), a beam with this radius would be highly mismatched (130% variation) in a wakefield driven by the Gaussian mode alone, and even though still small, the variation of the emittance is also larger for the mismatched beam ($\simeq 0.6\%$), due to the fact that the transverse tails of the electron beam distribution reach the nonlinear part of the focusing field. The higher-order mode uses twice the laser power and the matched spot size was increased by almost a factor of 3. When extrapolated to 3D, this implies that the charge of the beam can be increased by a factor of 9, or a gain of 4.5 in efficiency, for a given beam density and emittance.

The size of the electron beam is limited to the transverse region where the fields are linear, $|x/r_0| \lesssim 0.1$, in order to keep the emittance constant. To increase the region where the focusing fields are linear, more higher-order modes may be used to extend the flattop region of the laser pulse, with the condition that the beating of the modes of different orders is not significant. For example, using the first- and second-order Hermite-Gaussian modes with the fundamental, the flat region can be extended to $x/r_0 \simeq 0.2$, giving an additional factor of 2.5 gain in the beam radius.

D. Mitigation of laser mode beating

Two or more laser modes with parallel polarizations produce interference patterns (beating) in the intensity profile, as discussed in the previous section. In particular,

mode beating may be unavoidable in 3D, at least in one of the transverse planes, or if more than two modes are used. Considered next is the impact of mode beating and how it can be avoided in LPAs.

A fundamental and first-order Hermite-Gaussian mode propagating with parallel polarization produces mode beating. Near the axis, the beat term $\hat{a}_0 \hat{a}_1 \sim x \cos(k_{\text{beat}} z)$ produces a transverse force $F_d \sim a_0 a_1 \cos(k_{\text{beat}} z)$ that is nonzero on axis (assuming $k_{\text{beat}} \ll k_p$), i.e., a periodic deflecting force. Neglecting acceleration, the equation of motion for the transverse orbit of a highly relativistic electron is $d^2 x_e / dz^2 + k_\beta^2 x_e = F_d$, where $F_d = k_p E_{xd} / \gamma E_0$ is the normalized deflecting force and, near the axis, $E_{xd}/E_0 \simeq (4/k_p r_0) a_0 a_1 \phi_0 \sin(k_p \zeta) \cos(k_{\text{beat}} z)$. For an electron initially on axis, the transverse electron orbit is $x_e = F_{d0}(\cos k_{\text{beat}} z - \cos k_\beta z)/(k_\beta^2 - k_{\text{beat}}^2)$ for $k_\beta \neq k_{\text{beat}}$, and $x_e = (F_{d0}/2 k_\beta)(z \sin k_\beta z)$ for $k_\beta = k_{\text{beat}}$, where $F_{d0} = (4/\gamma r_0) a_0 a_1 \phi_0 \sin(k_p \zeta)$. Assuming that focusing is due to the fundamental Gaussian mode alone, $k_\beta^2 = (4/\gamma r_0^2) a_0^2 \phi_0 \sin(k_p \zeta)$, gives $F_{d0} = k_\beta^2 r_0 a_1 / a_0$. In the limit $k_{\text{beat}}^2 \ll k_\beta^2$, the amplitude of the transverse electron oscillation is $x_e \simeq r_0 a_1 / a_0$, which can be large. These transverse oscillations will be reduced when $k_{\text{beat}}^2 \gg k_\beta^2$. The condition $k_{\text{beat}}^2 \gg k_\beta^2$ implies $\gamma \gg (k r_0 a_0)^2 \phi_0 \sin k_p \zeta$, e.g., $\gamma \gg 5 \times 10^4$ (25 GeV) for $n_0 = 10^{17}$ cm^{-3} ($\lambda_p = 100$ μm), $\lambda = 0.8$ μm, $k_p r_0 = 3$, $a_0 = 1$, and $\phi_0 \sin k_p \zeta = 0.38$. The transverse orbit will be maximum at resonance, $k_{\text{beat}}^2 = k_\beta^2$, where secular growth will occur. This growth is large, e.g., after one-quarter betatron period $x_e = (\pi/4) r_0 a_1 / a_0$. However, if acceleration is included, the electron will quickly pass through this resonance (since $k_\beta \sim 1/\gamma$), limiting the growth. In general, such a transverse deflection force from the beating of parallel polarized modes should be avoided using one of the methods discussed in the following.

In LPAs, mode beating can be mitigated since laser pulses shorter than the plasma wavelength are used, e.g., $k_p L \lesssim 2$, and the wakefield response is determined by the intensity profile integrated over roughly a plasma period, as described by Eq. (16). Consider driving the wake by separating two short pulses (e.g., the lowest-order linear polarized mode and the lowest-order radially polarized mode) by a multiple of the plasma period $2\pi/\omega_p$. The pulses do not physically overlap, so there is no beating, but the wakefield behind the second pulse will have the structure of that driven by the sum of the intensity profiles of the two separate pulses. This is due to the fact that in the linear wakefield regime (and approximately in the quasi-linear regime), the wakefield driven by two separate pulses is a linear superposition of the two individual wakes.

Another method for mitigating the beating between modes in LPAs is to use two modes with different frequencies. Consider two modes with the same polarization but

different wave numbers k_{m_0,p_0} and k_{m_1,p_1}. The cross term in Eq. (14), without time averaging, has the form $a_{m_0,p_0} a_{m_1,p_1} \cos[(k_{m_0,p_0} - k_{m_1,p_1})\zeta + (\theta_{m_0,p_0} - \theta_{m_1,p_1})]$. Because the wake response is a result of a time integration of the laser intensity profile over the plasma period $2\pi/\omega_p$, for fast oscillations, $|k_{m_0,p_0} - k_{m_1,p_1}| \gg k_p$, the cross term averages to zero, yielding $\hat{a}^2 \simeq a_{m_0,p_0}^2/2 + a_{m_1,p_1}^2/2$, i.e., there is no intensity modulation. Note that because the wave numbers are different, the group velocities of the two modes will be different. To avoid too much separation of the two short-pulse modes over a long propagation distance, one should choose the two wave numbers sufficiently close. For example, requiring the slippage between the two modes over a dephasing length $L_d \sim \lambda_p k_{m_0,p_0}^2/k_p^2$ to be shorter than half a plasma wavelength, i.e., $|\beta_{g,m_0,p_0} - \beta_{g,m_1,p_1}| L_d < \lambda_p/2$, implies $|1 - k_{m_0,p_0}^2/k_{m_1,p_1}^2| < 1$, where β_g is the normalized group velocity and $4/k_p^2 r_0^2 \ll 1$ has been assumed. Satisfying the conditions $|1 - k_{m_0,p_0}^2/k_{m_1,p_1}^2| < 1$ and $|k_{m_0,p_0} - k_{m_1,p_1}| \gg k_p$ is facilitated by using lower plasma density, i.e., lower k_p.

Effectiveness of these techniques for control of the wake structure is demonstrated using 2D PIC simulations. Figure 9 shows the transverse electric field, as a function of distance behind the laser pulse, driven by a fundamental Gaussian pulse $(a_0 = 0.1)$ and a Hermite-Gaussian pulse $(a_1 = 0.07)$ in a matched plasma channel with $n_0 = 10^{19}$ cm^{-3} on axis, $k_p r_0 = 5.3$, and $k_p L = 2$. The resulting field when the pulses are crossed polarized (solid line) is compared to the resulting field when the pulses have parallel polarization but with the higher-order mode delayed by $2\pi/\omega_p$ (dashed line). Because the two pulses do not overlap, there is no modulation of the integrated intensity profile and the wakefield structure remains constant. Figure 9 also shows the transverse field when the two pulses have different frequencies $k_1 = 1.325 k_0$ (dash-dotted line). In all cases the driven fields are similar, although there is more variation ($\simeq 50\%$ at the first peak)
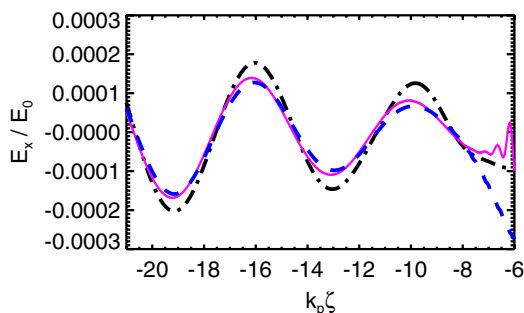
FIG. 9.   Transverse electric field driven by a Gaussian and a first-order Hermite-Gaussian pulse as a function of distance behind the laser, at $x/r_0 = 0.1$, with the two pulses having cross polarized (solid line), the Hermite-Gaussian mode delayed by $2\pi/\omega_p$ (dashed line), and different frequencies for the two pulses ($k_1 = 1.325 k_0$) (dash-dotted line).

when using different frequencies. In that case the field also varies more with propagation distance because of the greater difference of group velocity between the two components of the pulse, which can be reduced when operating at lower plasma density.

IV. CONCLUSION

In this paper the propagation of higher-order laser modes in plasma channels was studied with applications to LPAs. Solutions to the linear paraxial wave equation were presented for arbitrary order Hermite-Gaussian and Laguerre-Gaussian modes in Cartesian and cylindrical geometries for a laser pulse propagating in a plasma channel. Even though the condition for the matched propagation in a channel is the same for all modes (any mode can be propagated in the same density profile with the same matched spot size), the phase velocities for different modes vary (dependent on the mode number). For two or more modes copropagating in a channel with parallel polarization, the intensity profile becomes modulated due to an interference (beating) between the modes, with a modulation (beat) wavelength on the order of the Rayleigh length multiplied by a factor linearly dependent on the mode numbers. This can be avoided using orthogonally polarized modes. PIC simulations showed that these solutions hold over long propagation distances (many Rayleigh lengths) and at high intensities ($a_0 \sim 1$).

For LPAs, a combination of higher modes was used to control and/or reduce the wake focusing forces. In the linear wake regime (and approximately in the quasilinear wake regime), the focusing forces are linearly proportional to the transverse gradient of the laser intensity. Hence, by combining higher-order modes to produce an intensity profile that is transversely flat near the axis, the focusing force can be reduced to zero. The case of the fundamental Gaussian and the first-order Hermite-Gaussian mode with cross polarization in 2D Cartesian geometry was studied in detail. In particular, for an initially uniform plasma, conditions were found on the relative intensity of the two modes (a_1/a_0) for which the laser intensity profile is flat near axis, leading to zero focusing forces for all phases $k_p \zeta$ near the axis. When adding corrections due to a plasma channel, it was shown that while there is no condition where the focusing field gradient is constant (e.g., zero) for all phases near the axis, the two short-pulse modes can be shifted in time, and the relative intensity of the higher-order mode adjusted, such that the focusing field gradient stays constant near axis over a small interval in phase. By using this method, it is also possible to further control the shape of the focusing field longitudinally. In particular, the focusing field can be kept constant over a finite length in phase, i.e., the focusing field is constant over the length of the electron bunch and allows for some amount of phase slippage before the focusing force varies. These results were confirmed with 2D PIC simulations. Because the

two modes have different group velocities, the delay between them changes as they propagate and the condition for a flat focusing field is not exactly satisfied over a whole dephasing length. However, the focusing field can be significantly reduced compared to the response due to the two modes without initial delay.

Interference due to the beating of parallel polarized modes can occur in 3D and for cases involving more than two modes. Mode beating can lead to a component of the transverse wake that is nonzero on axis, i.e., a periodic transverse deflecting force with wave number k_{beat}. This deflecting force should in general be avoided, since it can lead to large transverse oscillations in the accelerated beam. The amplitude of the transverse beam oscillations is reduced when $k_{\text{beat}}^2 \gg k_{\beta}^2$, which will be the case at sufficiently high energies since $k_{\beta}^2 \sim 1/\gamma$. By using two modes of different frequencies, the beating becomes time dependent, and by choosing parameters such that the beat frequency is fast compared to the plasma frequency, the beat term essentially does not contribute to wake generation, i.e., there is no deflecting force. Alternatively, wake generation can be accomplished using two short-pulse modes that do not overlap in physical space, i.e., there is no beating.

Reduction of focusing forces is beneficial to LPAs since it can increase the matched beam radius of the accelerated electrons, in addition to reducing betatron oscillations and synchrotron radiation. The effects of reducing the focusing force on the accelerated electrons was examined using 2D PIC simulations. These simulations calculated the evolution of a test electron beam (zero charge) in a wakefield generated within a channel by higher-order laser modes in the quasilinear regime ($a_0 \sim 1$). It was shown that the matched beam radius is increased by a factor of 3, compared to using a fundamental Gaussian mode only, when the first-order mode is shifted in time relative to the fundamental mode. This corresponds to an increase of the beam charge and current by roughly a factor of 9 (for a flattop beam in 3D), without changing the peak density of the beam and for the same beam normalized emittance. The required laser power is increased by a factor 2 due to the addition of the higher-order mode. The beam radius, however, is limited to the region where the transverse field is flat, roughly, $\sigma_x/r_0 \lesssim 0.1$, beyond which nonlinear (x^3) contributions to the focusing forces become significant. More higher-order modes can then be added to extend the flat region of the wake to a larger transverse region about the axis.

The present work neglected the effects of beam loading and, similarly, simulations were performed using test electron beams. Beam loading (inclusion of the effects of the wake produced by the accelerated beam charge) can lead to significant distortions of the wakefield. In principle, a proper combination of higher-order modes can be found such that the beam-loaded wake can be flattened and/or controlled within the region of the accelerated beam. This will be a topic of future research.

APPENDIX: CODE BENCHMARKING

The evolution of an externally injected electron beam in the PIC code VORPAL [24] and in the 3D particle tracking code general particle tracer (GPT) [25], which has been shown to accurately model beam emittance evolution, are compared to assess the accuracy of the emittance calculation in the PIC code [34–36]. In GPT, the expressions for the longitudinal and transverse electric fields of the wake are described analytically in the low intensity limit ($a_0^2 \ll 1$), neglecting laser evolution and the channel contribution. The code GPT then evolves an electron beam in these specified fields. For comparison between the two codes, a case was chosen with low laser intensity ($a_0 = 0.1$). The laser pulse length is chosen so the excited wake is maximum ($k_p L = 2$, hence $E_{z_{\max}}/E_0 \simeq 0.0038$). The spot size of the laser pulse is $k_p r_0 = 7.6$ and the electron beam radius is $k_p \sigma_x = 0.72$ ($\sigma_x \sim 1.7$ μm with $n_0 = 5 \times 10^{18}$ cm^{-3}). The electron beam is composed of test particles, i.e., there are no space charge or beam loading effects.

Results are shown in Fig. 10, comparing a 2D PIC simulation with GPT, for an initial electron beam energy of 14 MeV ($\gamma = 28$). The initial normalized rms emittance is chosen so the electron beam spot size is matched, $\sigma_x^2 = (\epsilon_n r_0/2)(\gamma E_{z_{\max}}/E_0 \sin\theta)^{-1/2}$, hence $\epsilon_n = 0.07$ mm mrad. The beam is loaded at $\theta = 0.45$, where θ is the phase relative to the transverse wakefield [$E_x/E_0 \sim \sin(k_p \zeta + \theta)$], which corresponds approximately to the peak accelerating field. The dimensions of the simulation box for the PIC simulation are 67×108 μm with 4000×800 cells and four particles per cell for the background plasma. Figure 10 shows the evolution of the test electron beam spot size, normalized rms emittance, and
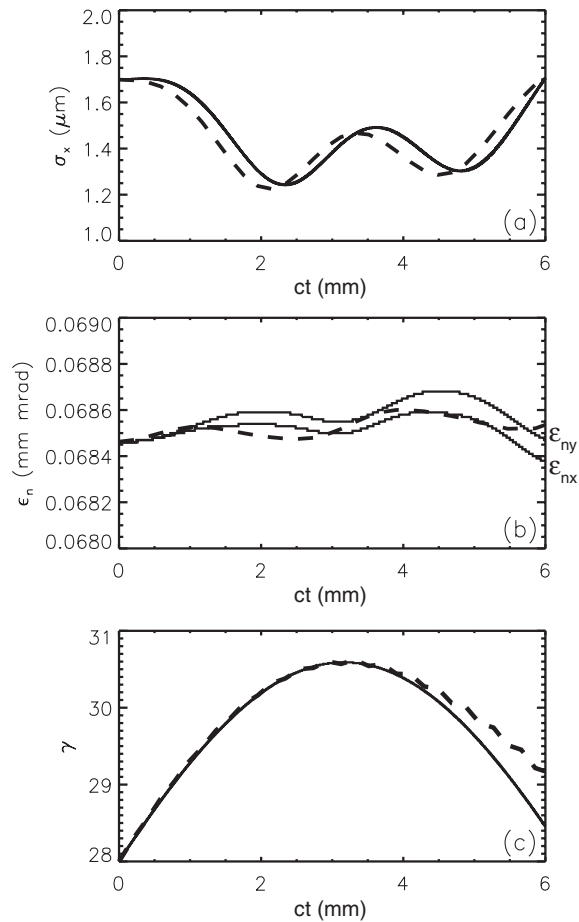
FIG. 10. Comparison between the PIC code VORPAL (dashed line) and the particle tracking code GPT (solid line) showing the evolution of a test electron beam (a) spot size, (b) emittance (in both transverse directions x and y for GPT), and (c) energy.

energy (γ). In Fig. 10(b) the two solid lines correspond to the measure of the normalized emittance in the two transverse dimensions x and y in GPT, the discrepancy between the two being due to particle statistics. There is in general a good agreement between the two codes. In particular, no artificial growth of the emittance is observed, which could arise from numerical noise, in the PIC simulation [34–36]. The beam radius oscillates (15% variation), due to a slight mismatch, at half the expected electron betatron wavelength $\lambda_\beta/2 = 3.7$ mm. The discrepancy in the electron beam radius evolution comes from the slight discrepancy of the phase between the transverse and longitudinal electric field due to the presence of the plasma channel in the PIC simulation. Note also that, because the beam is loaded in the first bucket after the laser pulse, to minimize the curvature effects due to the plasma channel in the PIC simulation, the field is different than the prescribed field in GPT when the beam slips into the region inside the laser pulse, leading to a different γ after dephasing.

The agreement is expected to be good in this case since a test electron beam is used, hence there is no noise expected

from the deposition of the beam particle current on the computational grid in the PIC simulation. Moreover, the beam is loaded in a region where the fields are linear, yielding to small errors in the interpolation of the fields to the beam particle positions.

[1] E. Esarey, P. Sprangle, J. Krall, and A. Ting, IEEE J. Quantum Electron. **33**, 1879 (1997).
[2] D. V. Korobkin, C. H. Nam, S. Suckewer, and A. Goltsov, Phys. Rev. Lett. **77**, 5206 (1996).
[3] H. M. Milchberg, C. G. Durfee, and T. J. McIlrath, Phys. Rev. Lett. **75**, 2494 (1995).
[4] E. Esarey, P. Sprangle, J. Krall, and A. Ting, IEEE Trans. Plasma Sci. **24**, 252 (1996).
[5] E. Esarey, C. B. Schroeder, and W. P. Leemans, Rev. Mod. Phys. **81**, 1229 (2009).
[6] G. V. Stupakov and M. S. Zolotorev, Phys. Rev. Lett. **86**, 5274 (2001).
[7] A. York, H. Milchberg, J. Palastro, and T. Antonsen, Phys. Rev. Lett. **100**, 195001 (2008).
[8] P. Michel, E. Esarey, C. B. Schroeder, B. A. Shadwick, and W. P. Leemans, Phys. Plasmas **13**, 113112 (2006).
[9] C. G. R. Geddes, C. Toth, J. van Tilborg, E. Esarey, C. B. Schroeder, D. L. Bruhwiler, C. Nieter, J. Cary, and W. P. Leemans, Nature (London) **431**, 538 (2004).
[10] C. G. Durfee and H. M. Milchberg, Phys. Rev. Lett. **71**, 2409 (1993).
[11] C. G. Durfee, J. Lynch, and H. M. Milchberg, Phys. Rev. E **51**, 2368 (1995).
[12] A. Zigler, Y. Ehrlich, C. Cohen, J. Krall, and P. Sprangle, J. Opt. Soc. Am. B **13**, 68 (1996).
[13] Y. Ehrlich, C. Cohen, A. Zigler, J. Krall, P. Sprangle, and E. Esarey, Phys. Rev. Lett. **77**, 4186 (1996).
[14] D. J. Spence, A. Butler, and S. M. Hooker, J. Phys. B **34**, 4103 (2001).
[15] W. P. Leemans, B. Nagler, A. J. Gonsalves, C. Tóth, K. Nakamura, C. G. R. Geddes, E. Esarey, C. B. Schroeder, and S. M. Hooker, Nature Phys. **2**, 696 (2006).
[16] C. B. Schroeder, E. Esarey, C. G. R. Geddes, C. Benedetti, and W. P. Leemans, Phys. Rev. ST Accel. Beams **13**, 101301 (2010).
[17] I. Kostyukov, A. Pukhov, and S. Kiselev, Phys. Plasmas **11**, 5256 (2004).
[18] W. Lu, C. Huang, M. Zhou, W. B. Mori, and T. Katsouleas, Phys. Rev. Lett. **96**, 165002 (2006).
[19] E. Esarey, B. A. Shadwick, P. Catravas, and W. P. Leemans, Phys. Rev. E **65**, 056505 (2002).
[20] P. Michel, C. B. Schroeder, B. A. Shadwick, E. Esarey, and W. P. Leemans, Phys. Rev. E **74**, 026501 (2006).
[21] J. B. Rosenzweig, B. Breizman, T. Katsouleas, and J. J. Su, Phys. Rev. A **44**, R6189 (1991).
[22] E. Cormier-Michel, C. G. R. Geddes, E. Esarey, C. B. Schroeder, D. L. Bruhwiler, K. Paul, B. Cowan, and W. Leemans, in *Advanced Accelerator Concepts*, edited by C. B. Schroeder, W. P. Leemans, and E. Esarey (AIP, New York, 2009), Vol. 1086, p. 297.
[23] J. B. Rosenzweig, A. M. Cook, A. Scott, M. C. Thompson, and R. B. Yoder, Phys. Rev. Lett. **95**, 195002 (2005).

[24] C. Nieter and J. R. Cary, J. Comput. Phys. **196**, 448 (2004).

[25] http://www.pulsar.nl/gpt.

[26] E. Esarey, P. Sprangle, J. Krall, A. Ting, and G. Joyce, Phys. Fluids B **5**, 2690 (1993).

[27] E. Esarey and W. P. Leemans, Phys. Rev. E **59**, 1082 (1999).

[28] C. G. R. Geddes, E. Cormier-Michel, E. Esarey, C. B. Schroeder, and W. P. Leemans, in *Proceedings of the 23rd Particle Accelerator Conference, Vancouver, Canada, 2009* (IEEE, Piscataway, NJ, 2009).

[29] B. A. Shadwick, C. B. Schroeder, and E. Esarey, Phys. Plasmas **16**, 056704 (2009).

[30] D. Umstadter, E. Esarey, and J. Kim, Phys. Rev. Lett. **72**, 1224 (1994).

[31] S. Dalla and M. Lontano, Phys. Rev. E **49**, R1819 (1994).

[32] G. Dugan, in *Advanced Accelerator Concepts*, edited by V. Yakimenko (AIP, New York, 2004), Vol. 737, p. 29.

[33] N. E. Andreev, L. M. Gorbunov, V. I. Kirsanov, K. Nakajima, and A. Ogata, Phys. Plasmas **4**, 1145 (1997).

[34] E. Cormier-Michel, B. A. Shadwick, C. G. R. Geddes, E. Esarey, C. B. Schroeder, and W. P. Leemans, Phys. Rev. E **78**, 016404 (2008).

[35] C. G. R. Geddes, E. Cormier-Michel, E. Esarey, K. Nakamura, G. R. Plateau, C. B. Schroeder, C. Toth, D. L. Bruhwiler, J. R. Cary, and W. P. Leemans, in *Advanced Accelerator Concepts*, edited by C. B. Schroeder, W. P. Leemans, and E. Esarey (AIP, New York, 2009), Vol. 1086, p. 12.

[36] C. G. R. Geddes, E. Cormier-Michel, E. H. Esarey, C. B. Schroeder, J-L. Vay, W. P. Leemans, D. L. Bruhwiler, J. R. Cary, B. Cowan, M. Durant, P. Hamill, P. Messmer, P. Mullowney, C. Nieter, K. Paul, S. Shasharina, S. Veitzer, G. Weber, O. Rubel, D. Ushizima, Prabhat, E. W. Bethel, and J. Wu, SciDAC Review **13**, 13 (2009).